Electro-Seismic Study Report

Lakes Oil Wombat Field, Gippsland Basin, Victoria, Australia

Processed for Lakes Oil on the 18th of July 2013

AQUATRONIC SOLUTIONS *Developers of Geophysical Equipment and Software*

Dr. Michael Du Preez

LAKES OIL N.L.

(A.B.N. 62 004 247 214) (A.C.N. 004 247 214)

Registered Office:
Level 14
500 Collins Street
Melbourne Vic. 3000
Telephone: (03) 9629 1566

Postal Address:
P.O. Box 300
Collins Street West
Melbourne Vic. 8007
Facsimile: (03) 9629 1624

19th September 2013

Mr John McKendry
Managing Director
Geothermal Mapping Limited
26 Emily Street
Gisborne 4010
New Zealand.

RE: APPROVAL TO PUBLICALLY RELEASE THE ATS REPORT(S) ON THE WOMBAT WELLS ELECTRO-SEISMIC SURVEY.

Dear John,

Approval is hereby granted to your company to publically release the results of the electro-seismic survey that was completed over the onshore tenement PRB 2 being the Wombat 1, 2, 3 and 4 wells, Gippsland Basin, Victoria, Australia for Lakes Oil LLC.

It certainly appears that this is very exciting technology. Given the survey was completed on a "blind' basis, Lakes Oil was very pleased with the results of this initial survey and we will be undertaking more electro-seismic surveys shortly.

Providing the Victorian Governments decision is favourable with regards to lifting the present well stimulation moratorium we will be submitting your report within our well stimulation applications. Given your report has determined the saline and fresh water aquifers beneath our site, that knowledge will assist us greatly with our environmental well stimulation designs and approvals.

We were very impressed with the high resolution and accuracy of your report and the low environmental foot print was a key component for Lake's Oil.

We look forward to working closely with your companies in the future.

Yours sincerely

Robert Annells
Chairman.

Table of Contents

1 Introduction

1.1 Background[22]

The first work done that contributed to the development of the electro-seismic effect was done in 1944 by Frenkel. He described the relative flow of fluid to the matrix brought about by the passage of a compression seismic wave through the medium. He investigated the induced electric fields generated by this relative motion of fluid, matrix interaction with Helmholtz-Smoluchowski equations. However, his investigations did not fully explain this relationship. In 1964, Biot made further progress by developing theories that predicted movement of a seismic wave through a saturated porous media. Various advances toward the development of a general equation describing the link between the relative fluid matrix interaction, and the electro-magnetic fields induced by this motion, were formulated between 1962 and 1994. These developments include irreversible thermodynamic coupling effects in porous media and averaging of fluid volume to determine the governing equations of the electro seismic effect. Then in 1995, Haartsen and Pride explained the electromagnetic field induced by the fluid motion relative to a porous matrix as being generated by dynamic current imbalances. These current imbalances are generated by plane sheer waves moving across and interface between rocks with different electro seismic properties. These net current imbalances induce an electromagnetic field which can be read at the surface as an interface response. However, if the plain sheer waves pass through a homogeneous saturated medium, with no interfaces of different electro kinetic properties, then the net currents induced will be balanced and cancel each other out. This essentially means there is no current flow induced by the relative motion of the fluid and matrix. This means no electromagnetic fields are induced that can be read at the surface. In 1997 Haartsen and Pride made use of their findings on electromagnetic interface response to investigate electro kinetic waves from single point sources in layered rock formations. They discovered saturated media interfaces produced a response equivalent to that of a dipole induced field on the interface directly under the seismic point source. In 1980, Chandler used a theoretical model and saturated core samples in laboratory experiments to relate the rise time of electro seismic signals to permeability. However, Haartsen in 1998 proved that the electro seismic response is a function of the salinity, porosity and permeability of a porous elastic media.

1.2 The electric double layer[6]

Grains of rock display net electric charges on their surfaces due to unsatisfied chemical bonds. In an aquifer, water makes contact with these charged surfaces and an electric potential is produced, since water is also electrolytic in nature. This potential difference then draws the free ions in the water toward the surface of the grain of rock where an electric double layer is formed. An electric double layer consists of a layer of ions drawn into the solid surface by electrostatic Van der Waal forces. This inner layer is called the Stern layer, while the outer layer consists of free ions in the water drawn in by the potential difference across the rock grain surface. This outer layer is called the Gouy layer. The Stern layer is only one ion thick and as shown in Figure 1, the electric potential drops sharply across this layer. Boltzmann distributions can be used to describe the concentrations of ions in the Gouy layer, provided that the electrolytic content in the water is lower than 0.1 moles per liter. The electric potential in this layer of diffused ions is described by the following equation:

$$\varphi(x) = \varphi_0 e^{-kx}$$

Where:

k = inverse Debye radius

x = distance from the charged surface

The slipping plane is the area where relative movement between the solid and water allow for motion between the outer diffused layer of ions and the inner strongly bound ions. This slipping plane has an electric potential across it that is called the zeta (ζ) potential. This electric potential is produced by the shearing between the inner and outer ions of the Stern and Gouy Layers. The Zeta potential plays an important role in the electro kinetic effect and is part of the equation used to determine the electromagnetic coupling tensor, which in turn determines the magnitude of the electromagnetic field induced.

1.3 The electro seismic effect[22]

The electro seismic effect can be observed when a fast traveling p wave intersects a water saturated interface of differing an-elastic or electrical properties. The electro seismic effect is in effect a form of converted energy which is released as dissipated energy. This conversion of energy takes place when a fast moving P waves produce slower P waves as it passes through the interface. These

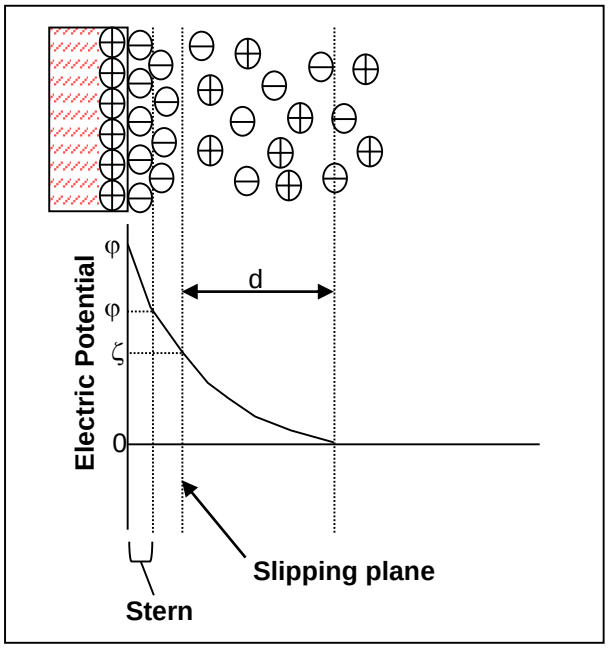

Figure 1 - Electric double layer[6]

slow P waves produce much more movement between the rock and water. This in turn leads to a high loss of energy in the form of heat due to friction and electro seismic effects, such as electromagnetic radiation due to ionic movement. Electro seismic signals are produced by the out of phase motion between all the ions in the water and those attached to the rock. The relationship between applied pressure *P* and electric potential response ϕ for a porous rock is generally given by the following equation (Millar and Clarke 1997):

$$\phi = -CP = -\left(\frac{\varepsilon\varepsilon_0\zeta}{\eta\sigma}\right)P$$

Where,

ϕ = electrical potential response or streaming potential

C = electro kinetic coefficient

P = applied pressure

$\varepsilon\varepsilon_0$ = permittivity of the pore space

ζ = zeta potential

η = fluid viscosity

σ = electrical conductivity

This equation relates the electrical potential response ϕ developed in a porous rock to the stimulus of an incident pressure change *P*, allowing the rock to be characterised by *C* on a macroscopic scale when modelling such electro kinetic responses. To see how the electro seismic function is derived please refer to Fourie's dissertation on electro-seismic field theory 2003[6].

1.4 Wave Behavior[22]

A seismic wave propagating in a medium can induce an electrical field or cause radiation of an electromagnetic wave. There are two electro-seismic effects that are considered in this report. The first effect is caused when a seismic wave crosses an interface between two media. When the spherical P-wave crosses the interface, it creates a dipole charge separation due to the imbalance of the streaming as shown in Figure 2. The second effect is caused when a seismic head wave travels along an interface between two media. It creates a charge separation across the interface, which induces an electrical field. This electric field moves along the interface with the head wave and can be detected by antennas when the head wave passes underneath as shown in Figure 3. Currents induced by the seismic wave on opposite sides of the interface. The electrical dipole radiates an EM wave which can be detected by remote antennas

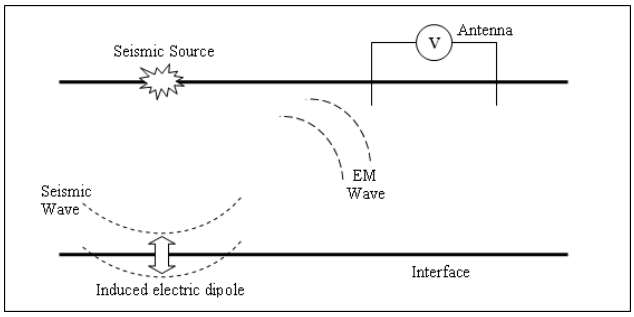

Figure 2 - Seismic wave crossing an interface generating an electromagnetic wave.

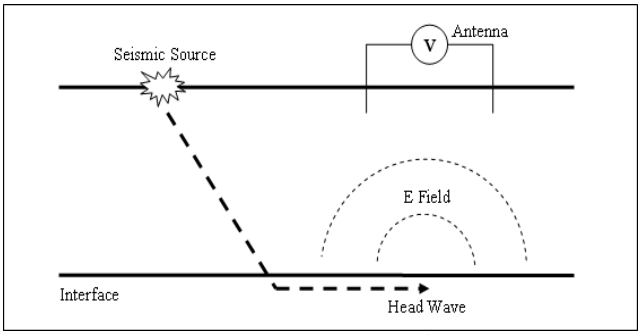

Figure 3 - Head wave travelling along an interface generating an electric field.

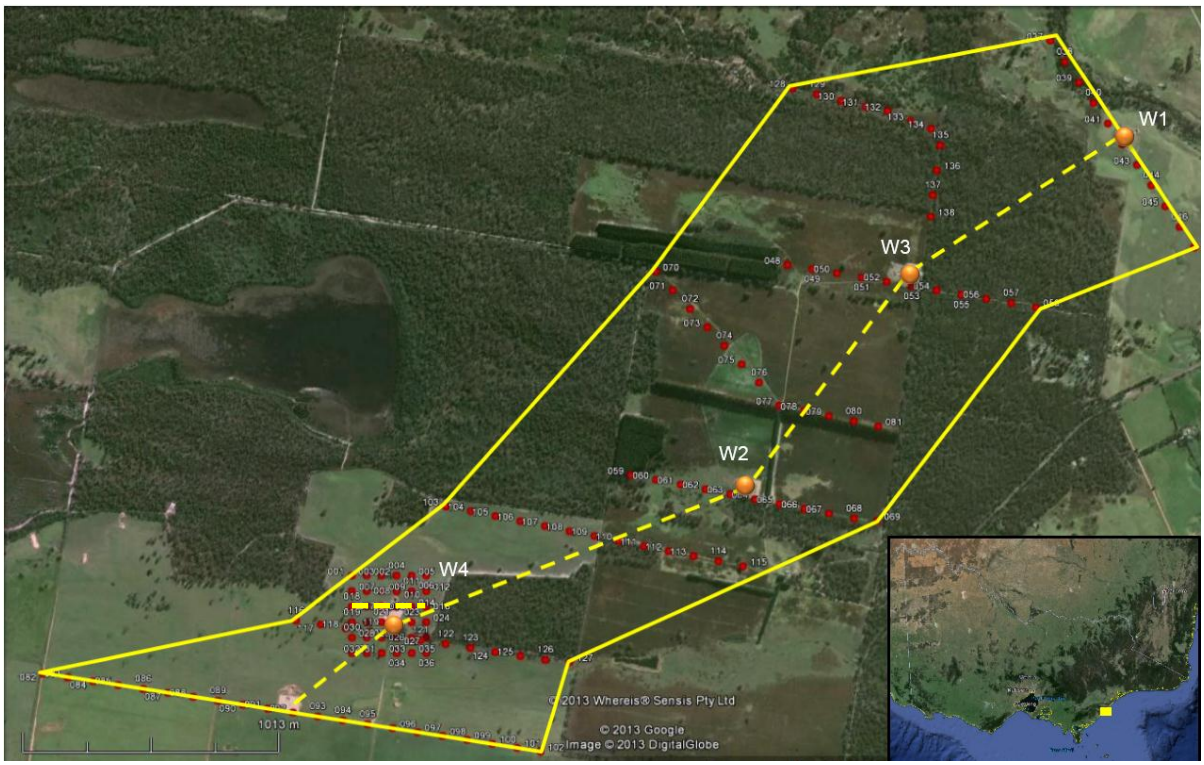

Figure 4 – Point positions

2 Site Description

The blind test site chosen for the study, provided by Lakes Oil, is located to the North of Seaspray, within the Gippsland Basin. The site was chosen due to the presence of four vertical wells drilled between 1500m and 2500m depth into the tight sands formations beneath the site. The locations and names of these wells, named W1, W2, W3 and W4, are shown on figure 4. Each of these wells have a full geological geological and lithological logs, as well as a set of downhole geophysical log sets in the Strzelecki Group tight sands. A full 3D seismic data set is also available over the site for comparitive data evaluation. A total of 138 survey points were sounded. These survey points can be seen on figure 4 and their co-ordinates, in WGS 84 lat long format, can be viewed in Table 1.

The electro-seismic survey area demarcated by a solid yellow line, shown on Figure 4, covers an area of 4.3 Km^2. The electro-seismic survey was conducted in eight profile intersects across the site, as shown in Figure 4. A smaller higher lateral resolution grid survey was also done around well W4. This survey grid was designed to allow for the generation of a 3D model of the sites electro-seismic responces. For the purposes of this paper, a comparative study is done for the transect line, shown by the dotted yellow line on Figure 4. This transect was chosen as it runs the length of the survey site and intersects each of the four vertical wells.

Table 1 – All points GPS(WGS84) positions

Point number	Northing	East
1	-38.3683	147.125
2	-38.3683	147.1257
3	-38.3683	147.1264
4	-38.3683	147.127
5	-38.3683	147.1277
6	-38.3683	147.1284
7	-38.3688	147.125
8	-38.3688	147.1257
9	-38.3688	147.1264
10	-38.3688	147.1271
11	-38.3688	147.1277
12	-38.3688	147.1284
13	-38.3694	147.1284
14	-38.3694	147.1277
15	-38.3694	147.1271
16	-38.3694	147.1264
17	-38.3694	147.1257
18	-38.3694	147.125
19	-38.3699	147.125
20	-38.3699	147.1257
21	-38.3699	147.1264
22	-38.3699	147.1271
23	-38.3699	147.1277
24	-38.3699	147.1284
25	-38.3705	147.1284

26	-38.3705	147.1277
27	-38.3705	147.1271
28	-38.3705	147.1264
29	-38.3705	147.1257
30	-38.3705	147.125
31	-38.371	147.125
32	-38.371	147.1257
33	-38.371	147.1264
34	-38.371	147.1271
35	-38.371	147.1277
36	-38.371	147.1284
37	-38.3492	147.1568
38	-38.3499	147.1575
39	-38.3507	147.1581
40	-38.3514	147.1588
41	-38.3521	147.1594
42	-38.3529	147.1601
43	-38.3536	147.1608
44	-38.3543	147.1614
45	-38.3551	147.1621
46	-38.3558	147.1627
47	-38.3566	147.1634
48	-38.3572	147.1448
49	-38.3573	147.1459
50	-38.3575	147.1471
51	-38.3576	147.1482
52	-38.3578	147.1493
53	-38.358	147.1505
54	-38.3581	147.1516
55	-38.3583	147.1527
56	-38.3584	147.1539
57	-38.3586	147.155
58	-38.3587	147.1561
59	-38.3647	147.1377
60	-38.3649	147.1388
61	-38.365	147.14
62	-38.3652	147.1411
63	-38.3654	147.1422
64	-38.3655	147.1433
65	-38.3657	147.1445
66	-38.3659	147.1456
67	-38.3661	147.1467
68	-38.3662	147.1478
69	-38.3663	147.1489
70	-38.3574	147.1388
71	-38.3581	147.1396
72	-38.3588	147.1404
73	-38.3594	147.1412
74	-38.3601	147.1419
75	-38.3607	147.1427
76	-38.3614	147.1435
77	-38.3622	147.1444
78	-38.3624	147.1456
79	-38.3626	147.1467
80	-38.3628	147.1478
81	-38.3629	147.1489
82	-38.3717	147.111
83	-38.3719	147.1121
84	-38.372	147.1133
85	-38.3722	147.1144
86	-38.3723	147.1155
87	-38.3724	147.1167
88	-38.3726	147.1178
89	-38.3727	147.1189
90	-38.3729	147.1201
91	-38.373	147.1212
92	-38.3731	147.1223
93	-38.3733	147.1235
94	-38.3734	147.1246
95	-38.3736	147.1257
96	-38.3737	147.1269
97	-38.3738	147.128
98	-38.374	147.1291
99	-38.3741	147.1303
100	-38.3743	147.1314
101	-38.3744	147.1325
102	-38.3745	147.1336
103	-38.3658	147.1293
104	-38.366	147.1304
105	-38.3661	147.1315
106	-38.3663	147.1327
107	-38.3665	147.1338
108	-38.3667	147.1349
109	-38.3669	147.136
110	-38.367	147.1372
111	-38.3672	147.1383
112	-38.3674	147.1394
113	-38.3676	147.1405
114	-38.3677	147.1417
115	-38.3679	147.1428
116	-38.3699	147.1225
117	-38.37	147.1236
118	-38.3701	147.1247
119	-38.3703	147.1259
120	-38.3704	147.127
121	-38.3706	147.1281
122	-38.3707	147.1293
123	-38.3708	147.1304
124	-38.371	147.1315
125	-38.3711	147.1327
126	-38.3713	147.1338
127	-38.3713	147.1349
128	-38.3509	147.145
129	-38.3511	147.1462
130	-38.3513	147.1473
131	-38.3515	147.1484
132	-38.3517	147.1494
133	-38.3521	147.1504
134	-38.3523	147.1514
135	-38.3529	147.1518
136	-38.3538	147.1516
137	-38.3547	147.1514
138	-38.3555	147.1513

3 Site Conditions

The wombat site had four inches of rain the week before the survey commenced, as such the site top soil was softer than expected. This impacted on the maximum survey depth, which was limited to 3000m, due to acoustic absorption of the seismic impulse source wave in the soft top soils.

There were problems accessing three survey point locations at points 37, 38 and 58. As such these points were not surveyed.

The nature of the site prevented the use of straight regular grid lines as the authors were forced to conduct soundings on the currently existing tracks and open fields to avoid environmental impact.

4 Seismic Source Equipment

In order to collect electro-seismic data to a depth of 3000m, a weight drop impulse seismic source was utilised. The weight drop consists of a 250 kg dropped from a height of 3.5m above surface level.

Since the site top soil conditions on site was soft, a large 50cm by 50cm base plate was used to limit soil compaction in an attempt to inject more seismic energy into the ground. This approach did help, however, some sounding locations were still not ideal.

A 20 point stacking strategy was used to improve sounding signal to noise ratio and to improve sounding redundancy.

5 Project Objectives

The study objectives at the outset of the project were as follows:

- Define the aquifer systems under the site
- Define the primary permeability of the aquifers under the site
- Define secondary permeability of the aquifers under the site
- Define any aquiclude formations under the site
- Define any possible structures, such as dykes, faults and sills that may affect the hydro-geology of the site
- Define any secondary permeability caused by such faulting or intrusive formations
- Define the coal measure formations under the site
- Define the tight sands formation under the site
- Define the known weathered sands formation above the tight sand formation
- Define any oil reserve formations under the site
- Define any possible groundwater influx zones at depth

6 Model Calibration

The data discussed in this report was calibrated against the provided geological well log data and seismic velocity profiles provided by Lakes Oil for wells W1 through 4.

Hydraulic Conductivity data was also calibrated against the core sample analysis permeability data provided by Lakes oil for samples at discrete depths and is expressed in mm/day. As full permeability logs were not available for the wells, the ES hydraulic conductivity data for the remaining ES data was calibrated against a linear depth variant model calibrated at discrete depth points.

7 Model Assumptions

The following assumptions were made when developing the site geological model.

- A low resolution grid survey of 100m inter-point spacing and approximately 500m interline spacing, was used investigate the site. This limits the survey to a general overview of the aquifer, geological, and oil reserve systems.
- Due to the inclining geology under the investigation site, there are seismic velocity variances of up to 10% of total depth.
- The analysis of fractures under the site is assumed to be bedding plain in nature. Fractures with a dipping angle of more than 30 degrees are not typically seen in ES studies.
- Due to the low resolution grid utilised the interpolation methods used, in generating the model and 2D section, is biased in the horizontal plain resulting in a reduction of vertical resolution of dipping geological formations.

8 Site Geology and Lithology[21]

Figure 5 shows an overview of the site geology as interpreted by Lakes Oil. The geological overview indicates that the site consists of eight major formations. The upper most formation is the Quaternary – Upper Miocene sands and gravels which house the shallow aquifer which is used across the area. This is followed by the Tambo River Formation then the Gippsland limestone formation which holds some aquifer potential. This is followed by the Lakes Entrance formation which is also an aquitard in nature and consists primarily of Marls. The Latrobe Group formation follows this and consists of sands and coals. There are two distinct coal beds indicated on Figure 5. To the east of the site there is a sub-group formation called the Emperor formation which is underlain by volcanic basalts. To the west, these formations are not seen and are instead replaced by a weathered Strzelecki formation. This weathered formation consists of permeable sands. The un-weathered Strzelecki formation below this is the same formation as the weathered Strzelecki formation and consists of tight sands. Both the weathered and un-weathered Strzelecki contain gas bearing tight sands.

9 Electro-Seismic Investigation

The 3D model tree, accessible in Acrobat reader 8.1 or higher by selecting the tree icon to the left of the model view space, allows for the selection of the 3D volume data for the individual model data sets. The basic model options show the:

- Bounding Box – The limits of the low resolution model
- North arrow – Which shows the direction of north
- Map – Which shows a site plan and survey point positions
- Map Bottom - Which shows the same map at the bottom of the model boundary
- 2d Layer lines – which show the positions of the 4 wells on the site
- 2D layer – Which shows the model axis text
- Fine Grid bounding box – Which shows the boundaries of the high resolution grid around Wombat 4

9.1 Hydraulic Conductivity Tomography (ESKT)[22]

Figure 6 shows the electro seismic hydraulic conductivity tomography study results for the investigation site cross section profile. The data is expressed as hydraulic conductivity values from 1 to 0 mm/day. This scale was chosen to visually enhance the lower permeability formations in the tight sands at depth. As such, the aquifer systems in the top 100m are over emphasized. The hydraulic conductivity values shown in Figure 6 are modelled estimates of the sites formation permeability's as no absolute hydraulic conductivity values are available for the site.

The 3D model tree, accessible in Acrobat reader 8.1 or higher by selecting the tree icon to the left of the model view space, allows for the selection of the 3D volume data for the individual model data sets. The Hydraulic conductivity data is selected by selecting the "Hydraulic conductivity 0.5 mm/day" option on the model tree. This data shows the 3D volume data for the Hydraulic conductivity of the site at a value of 0.5mm/day.

The Hydraulic conductivity data for the sands of the Strzelecki Formation is selected by selecting the "Sands Hydraulic conductivity 0.05 mm/day" option on the model tree. This data shows the 3D volume data for the Strzelecki sands Hydraulic conductivity of the site at a value of 0.05mm/day.

The Hydraulic conductivity Section data at a depth of 1370m is selected by selecting the "Section 1370" option on the model tree. This data shows the 2D horizontal section data for the horizontal Hydraulic conductivity of the site at a depth of 1370m for a value scale of 0.05mm/day to 0mm/day.

The Hydraulic conductivity Section data at a depth of 1150m is selected by selecting the "Section 1150" option on the model tree. This data shows the 2D horizontal section data for the horizontal Hydraulic conductivity of the site at a depth of 1150m for a value scale of 0.05mm/day to 0mm/day.

9.2 Electro Seismic Coupling Coefficient Tomography (ESCCT)[22]

Figure 8 shows the electro seismic coupling coefficient tomography data for the site. The ESCCT data is representative of the electrical characteristics that define the interaction between the pressure waves to electrical field conversion. The ESCCT data is expressed as a percentage of conversion. The data can be used as indicators for salinity variations within an aquifer system. In hydro-carbon studies ESCCT data can be used to delineate the high salinity fluids associated with hydro-carbon reservoirs. Variations of ESCCT data within target hydro-carbon reservoirs can indicate the presence of hydro-

carbons, due to viscosity variation effects on the ESCCT responses.

The 3D model tree, accessible in Acrobat reader 8.1 or higher by selecting the tree icon to the left of the model view space, allows for the selection of the 3D volume data for the individual model data sets. The ES Coupling coefficient data is selected by selecting the “Potential oil reserves” option on the model tree. This data shows the 3D volume data for the ES coupling coefficient information under the site at a value of 99 % coupling. The value is set very high in order to visualise only the very highest ESCCT values under the site which is representative of the potential oil reserves under the site.

9.3 Fracture Analysis (ESFT)[22]

The fracture analysis tomography results shown in Figure 8 for the test profile show the inferred fracture zone depths. The electro seismic data is spectrally analysed and specific frequency patterns associated with fracturing are used to infer fracturing with depth. The results shown in Figure 8 are used to show secondary permeability within a primary permeability aquifer. These fractured zones are associated with higher fluid flow rates. Electro-seismic sounding methods can only delineate bedding plain fracturing with a maximum tilt of 30 degrees to the horizontal plain. The fracture data indicated in Figure 8 is an interpolated representation of the potential fracture zones under the site and is not representative of the shape, tilt, pitch, strike and lateral extent of individual fractures. To clearly define a fracture network, a far higher survey grid resolution would be required.

The 3D model tree, accessible in Acrobat reader 8.1 or higher by selecting the tree icon to the left of the model view space, allows for the selection of the 3D volume data for the individual model data sets. The Fracture data is selected by selecting the “Bedding Plain Fracturing” option on the model tree. This data shows the 3D volume data for the Fracture surfaces under the site.

The Fracture data for the high resolution grid survey is selected by selecting the “Fine Grid Bedding Plain Fractures” option on the model tree. This data shows the 3D volume data for the high resolution grid Fracture surfaces around the Wombat 4 well.

9.4 Electro-Seismic Change in Absolute Gradient Response Tomography (ESCAGT)

Figure 6 also shows the electro seismic change in absolute gradient response which is used to differentiate absolute electrical changes in rock formation properties, in proportion to each other. This method allows the user to discern formation changes of similar electrical characteristics and when used in conjunction with the electro seismic permeability response tomography, provides deeper insight into the geological and lithological information for subsurface formations. It is also used to support the delineation of subsurface faulting and intrusive formations not from an interface standpoint but rather from an absolute electrical standpoint.

The 3D model tree, accessible in Acrobat reader 8.1 or higher by selecting the tree icon to the left of the model view space, allows for the selection of the 3D volume data for the individual model data sets. The Change in absolute gradient response data is selected by selecting the “Structure analysis data” option on the model tree. This data shows the 3D volume data for the Change in absolute gradient response of the site at a value of 10% gradient change. This volume defines the ES responses related to the coal seam formations under the site.

The interpreted formation horizons generated by the analysis of the ESCAGT data is selected by selecting the “Formation Horizon” option on the model tree. This data shows the 3D surface data horizons for the interpreted coal bed horizons under the site.

9.5 Electro-Seismic Groundwater Flow Potential Tomography (ESGFPT)

The ESGFPT data shown in Figure 10 indicates areas under the investigation site which may produce significant amounts of groundwater influx into a drilled well. The data takes into account primary and secondary permeability as well as electro-seismic gradient response and fracture network interpretations to determine potential groundwater high flow regions.

The 3D model tree, accessible in Acrobat reader 8.1 or higher by selecting the tree icon to the left of the model view space, allows for the selection of the 3D volume data for the individual model data sets. The Groundwater flow potential data is selected by selecting the “Potential inflow structures” option on the model tree. This data shows the 3D volume data for the Groundwater flow probability of the site at a value of 10% probability.

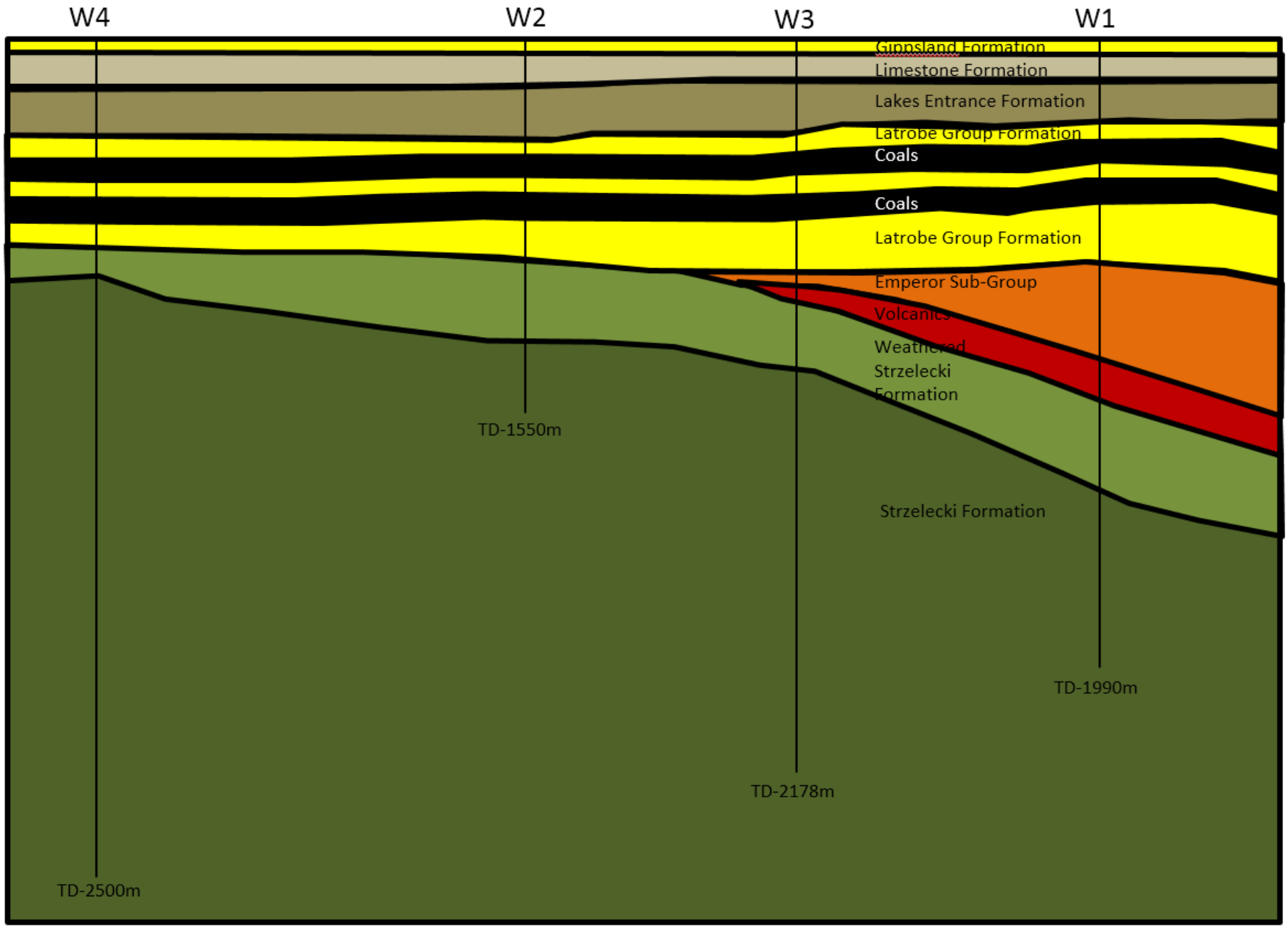

Figure 5 – Site geological overview (Lakes Oil)

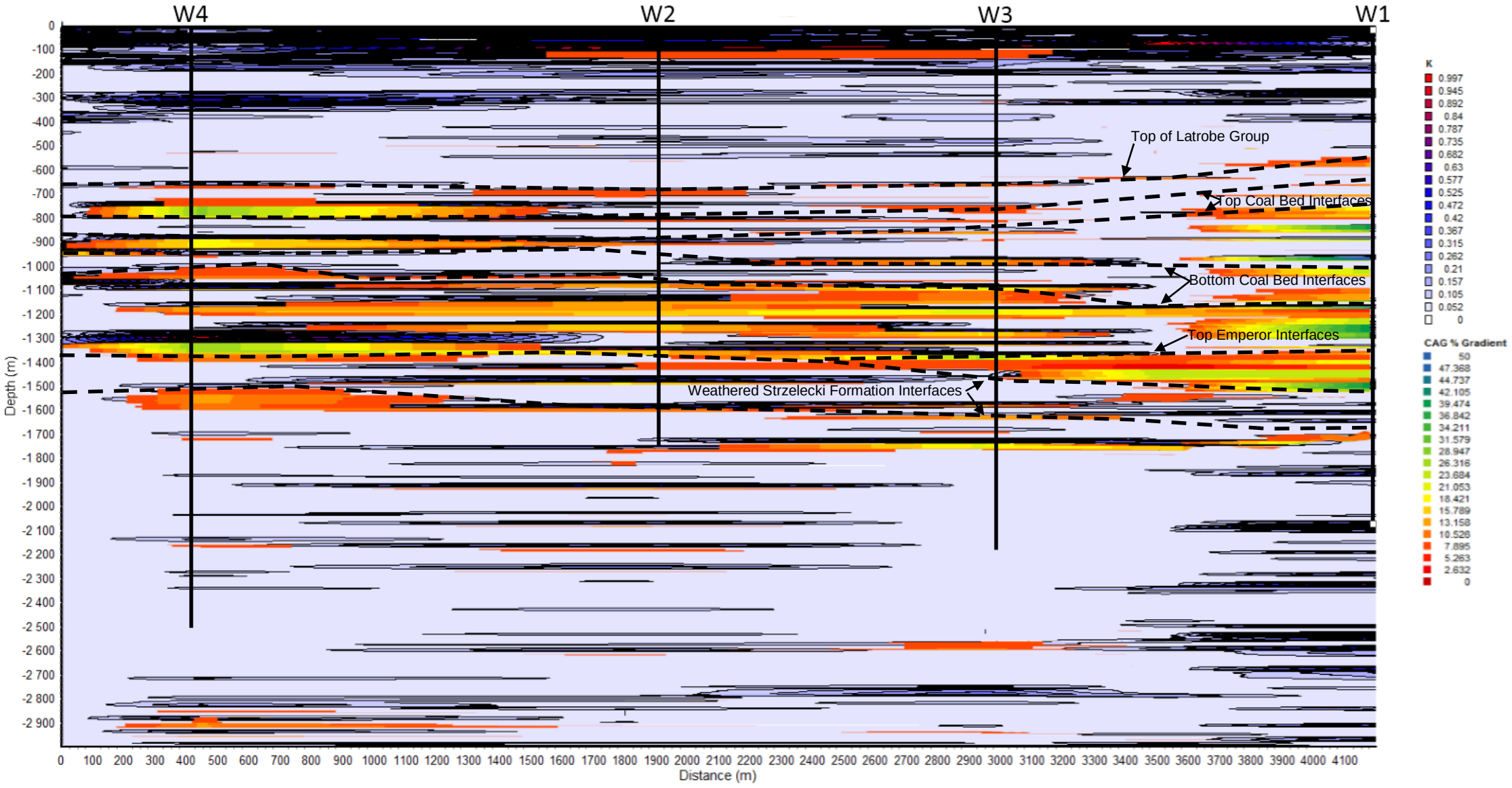

Figure 6 – ES Permeability and ESCAGT Response

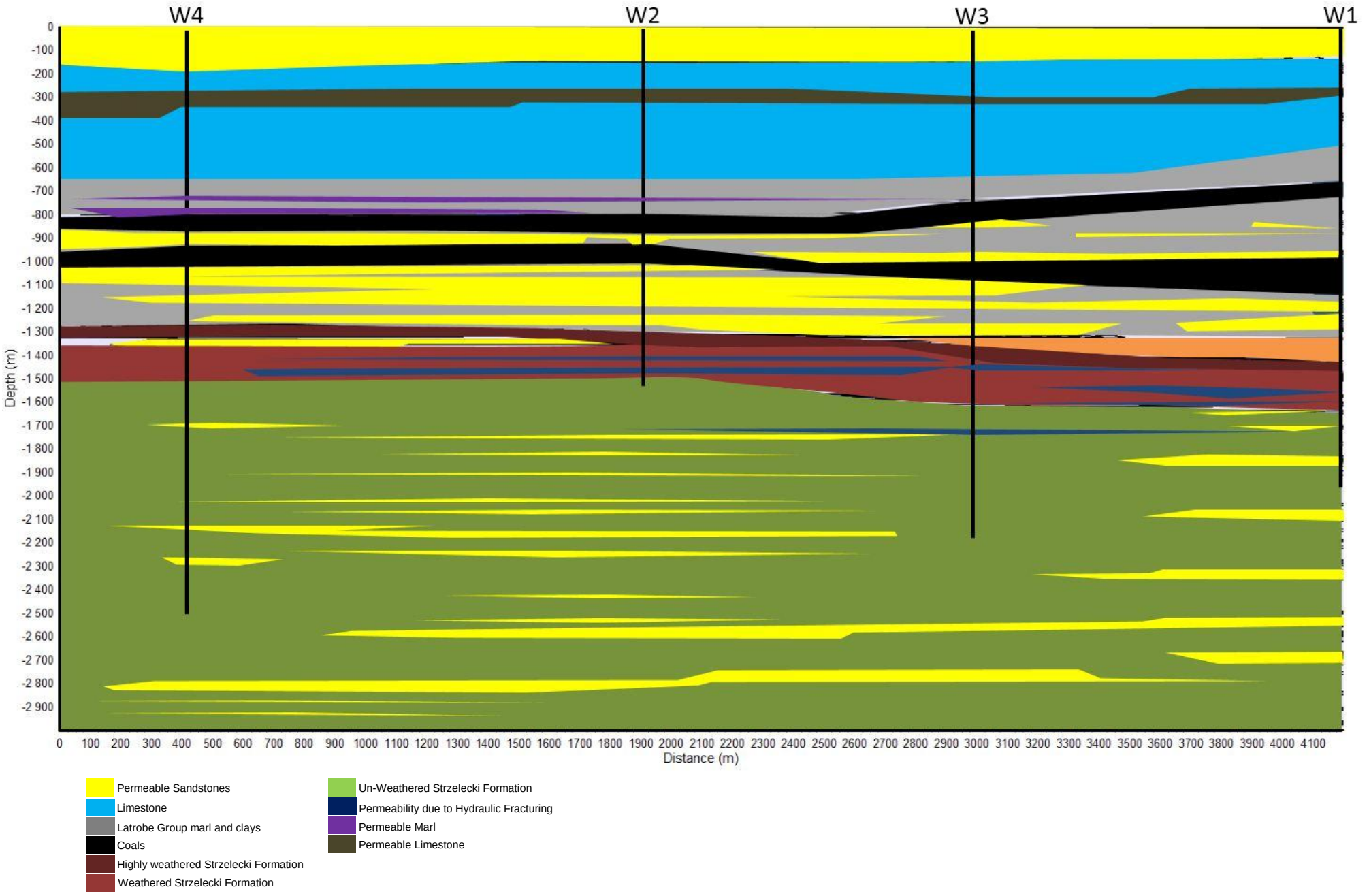

Figure 7 – ES Site geological interpretation

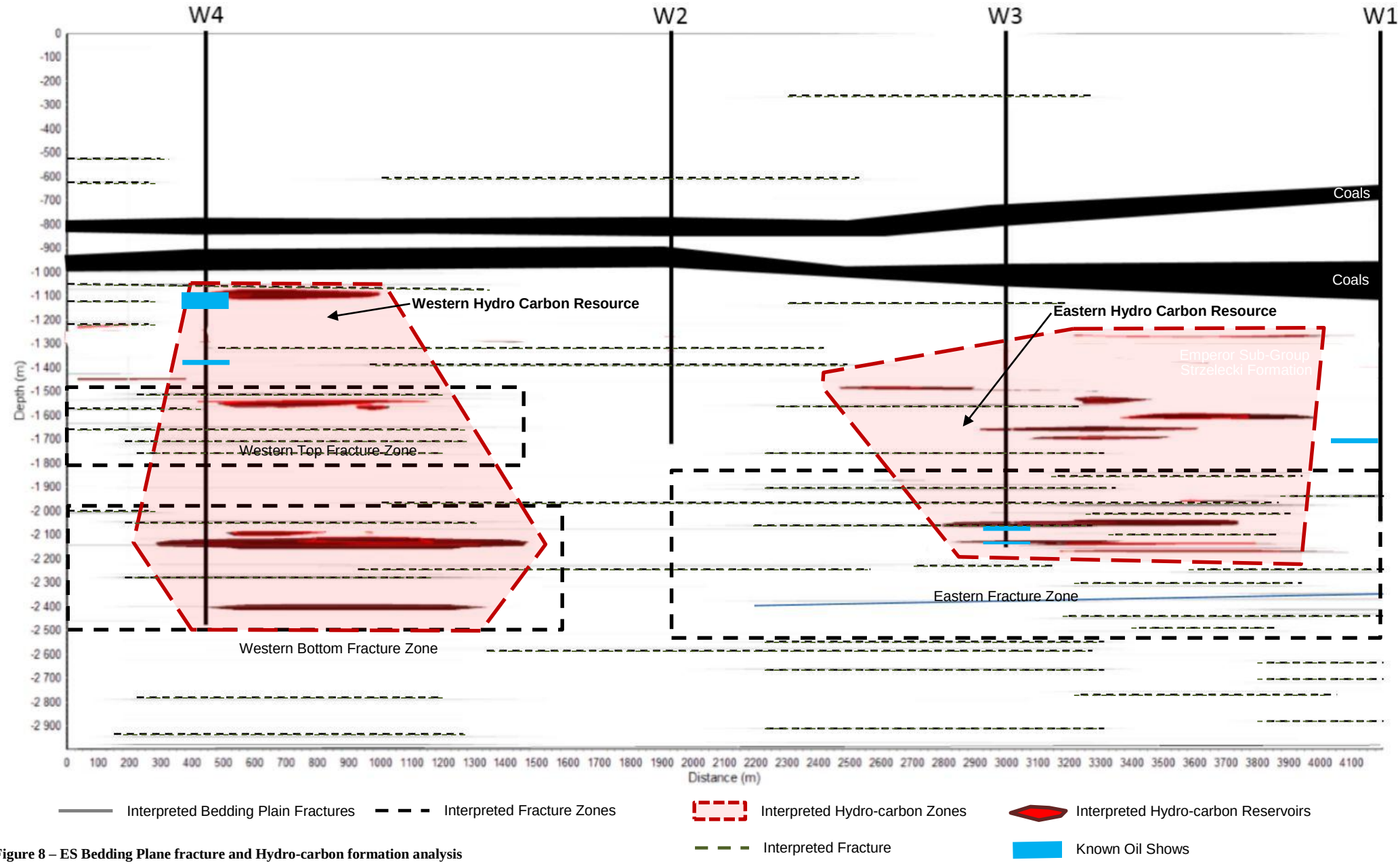

Figure 8 – ES Bedding Plane fracture and Hydro-carbon formation analysis

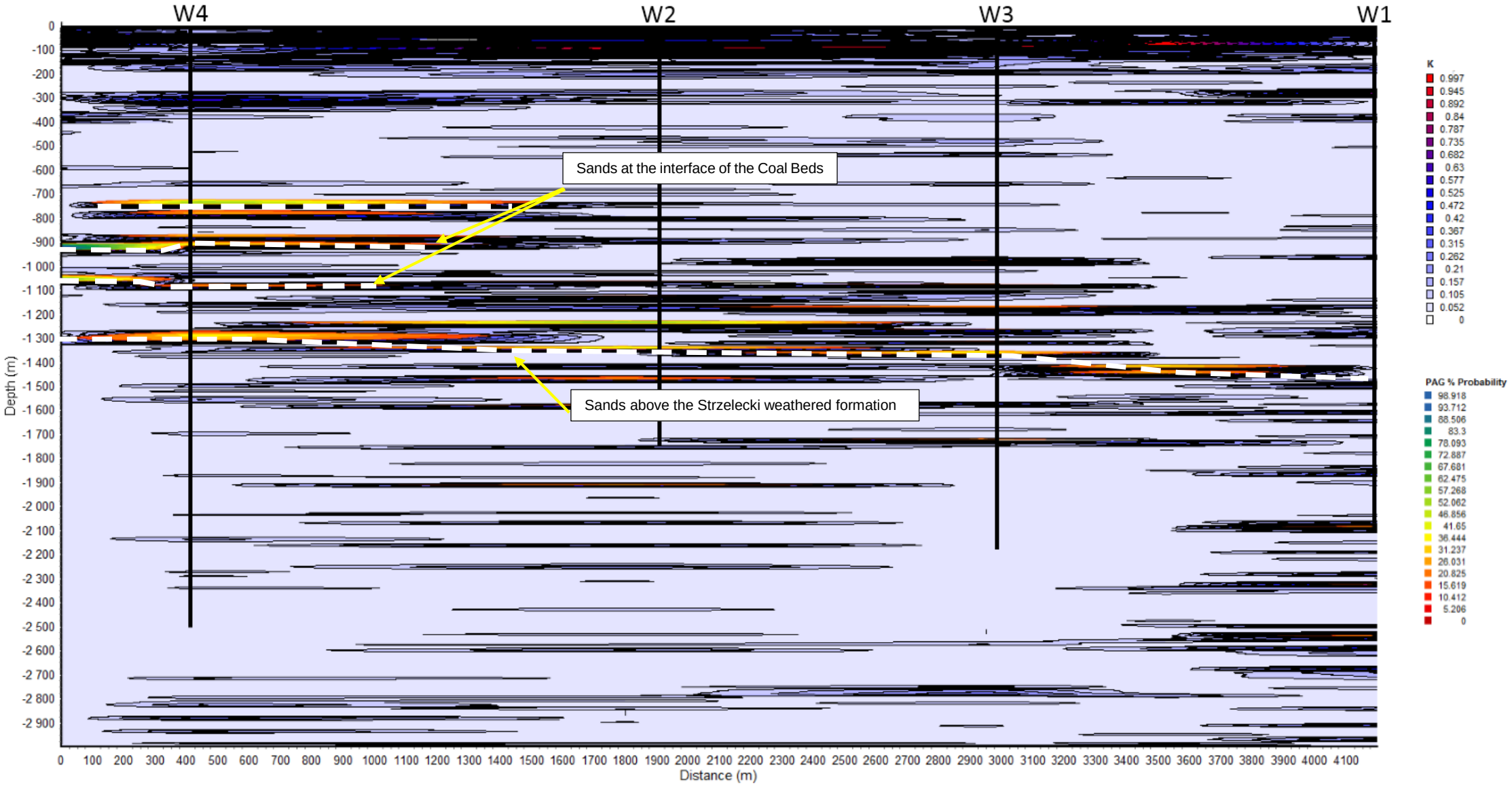

Figure 9 – ES Groundwater Flow Potential (ESGFPT)

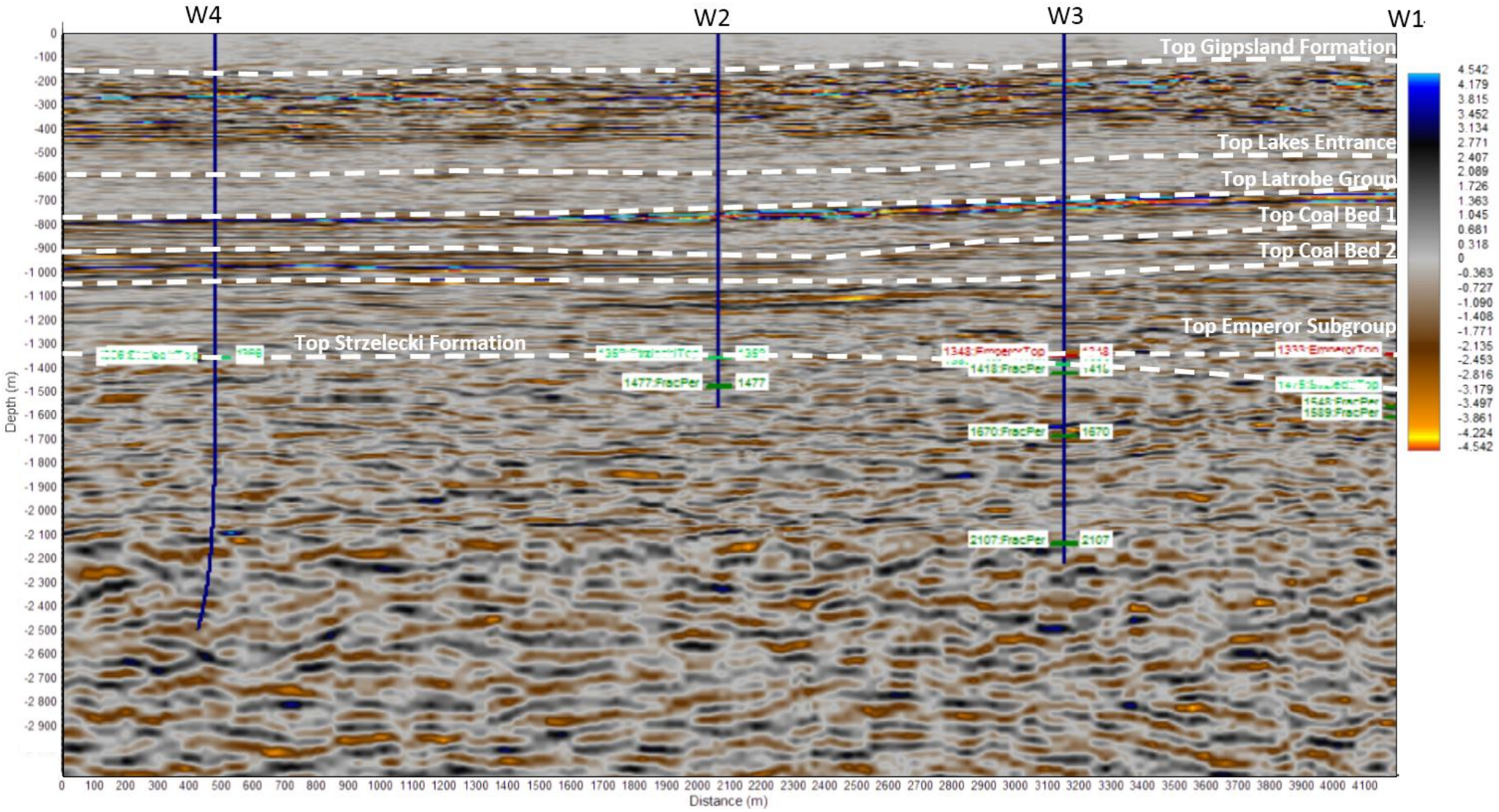

Figure 10 –2D Seismic section and formation interface interpretation

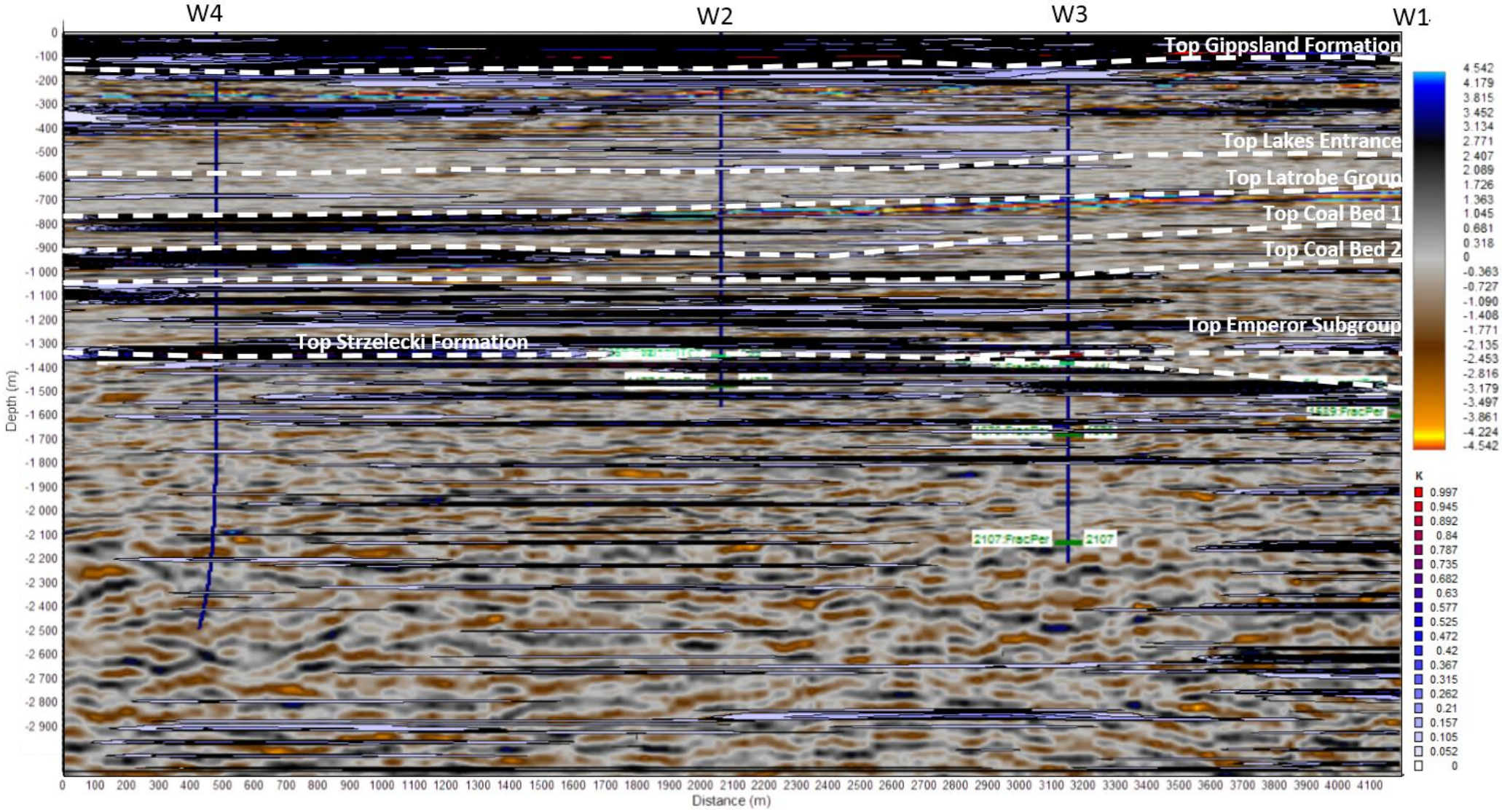

Figure 11 – ES Hydraulic Conductivity (ESK) to Seismic section and formation interface interpretation comparison

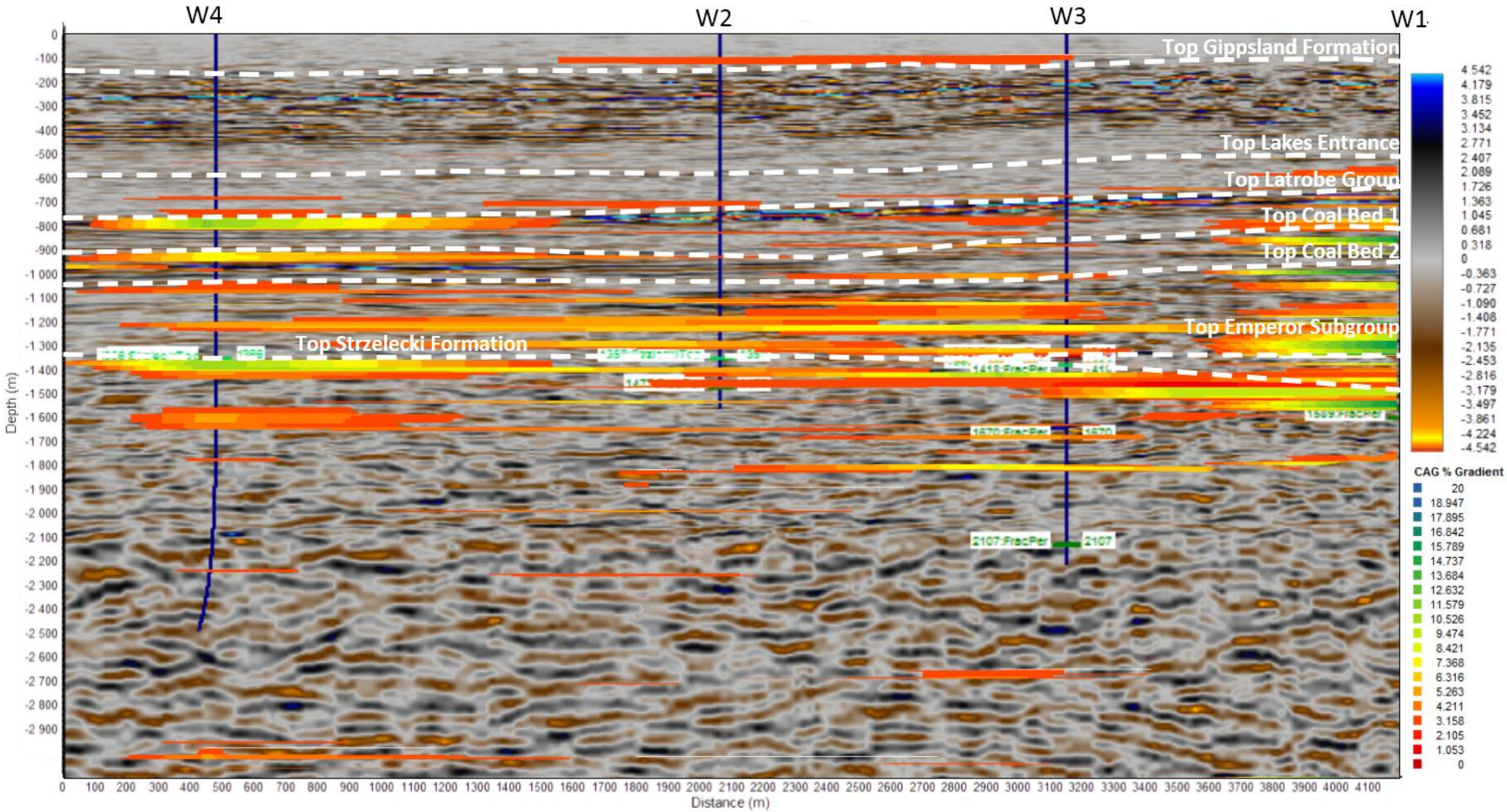

Figure 12 – ES Change of Absolute Response Gradient (ESCAGT) to Seismic section and formation interface interpretation comparison

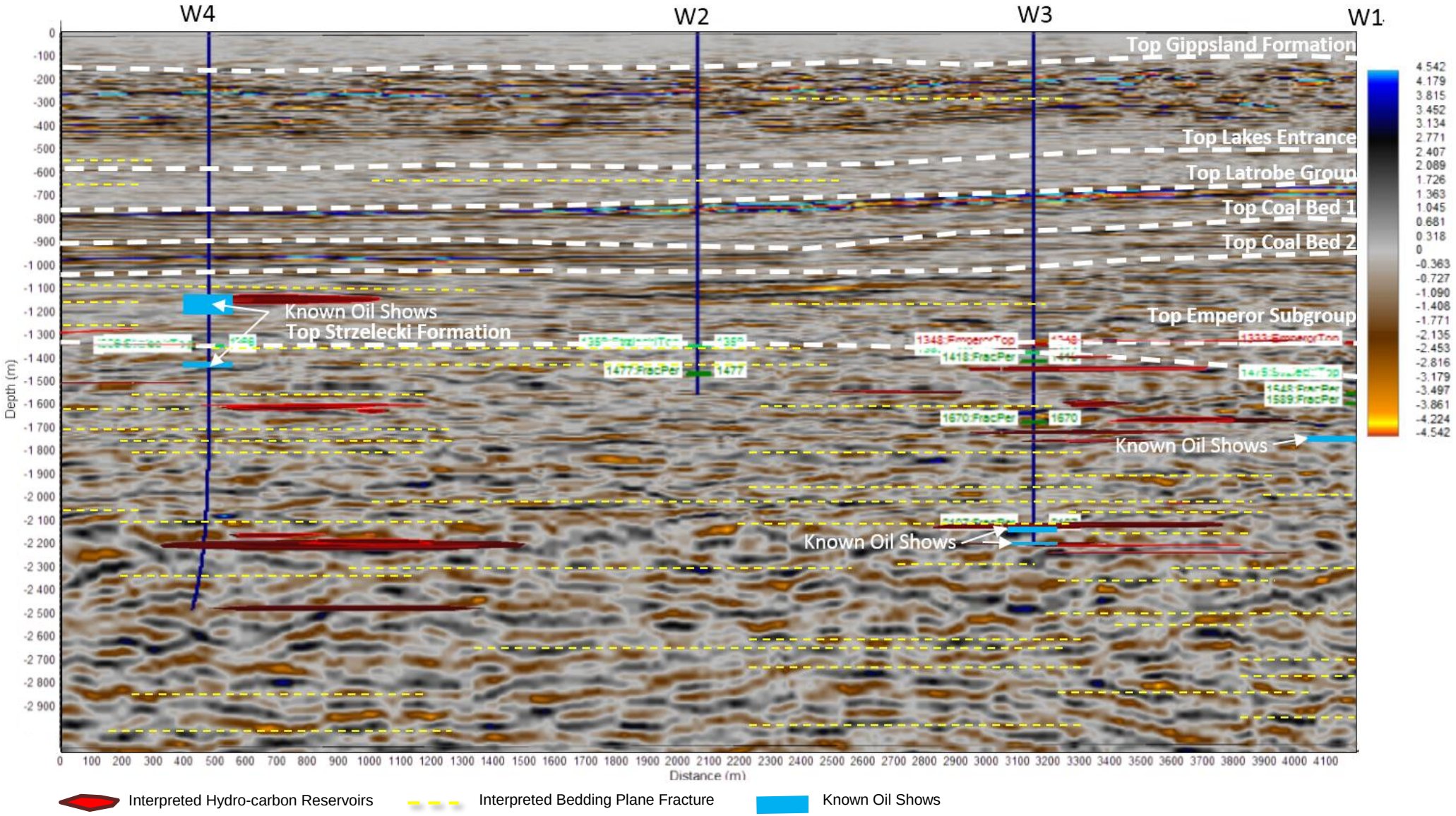

Figure 13 – ES Fracture (ESFT) and ES Coupling Coefficient (ESCCT) to Seismic section and formation interface interpretation comparison

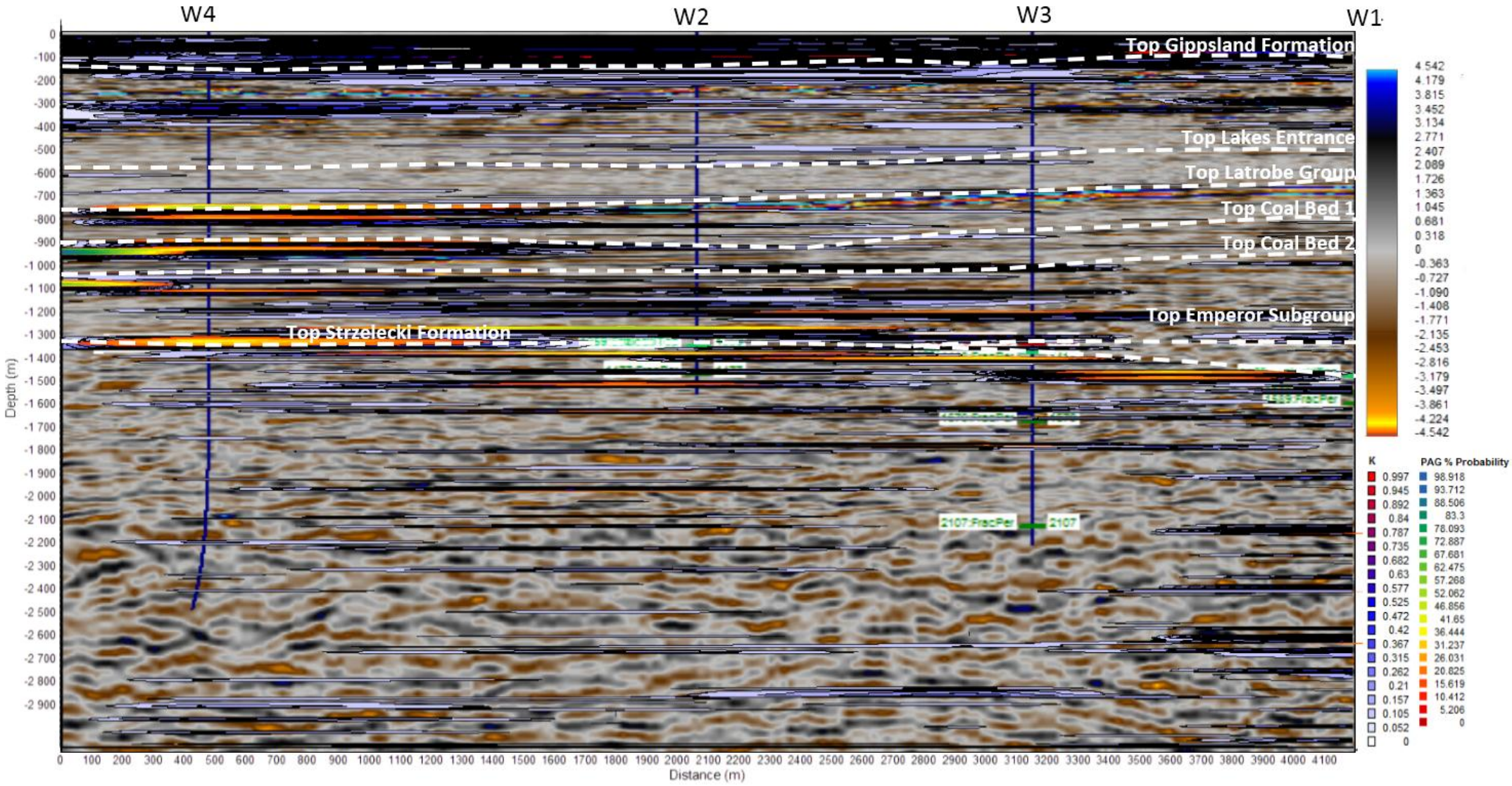

Figure 14 – ES Hydraulic Conductivity (ESKT) and ES Groundwater Flow Potential (ESGFPT) to Seismic section and formation interface interpretation comparison

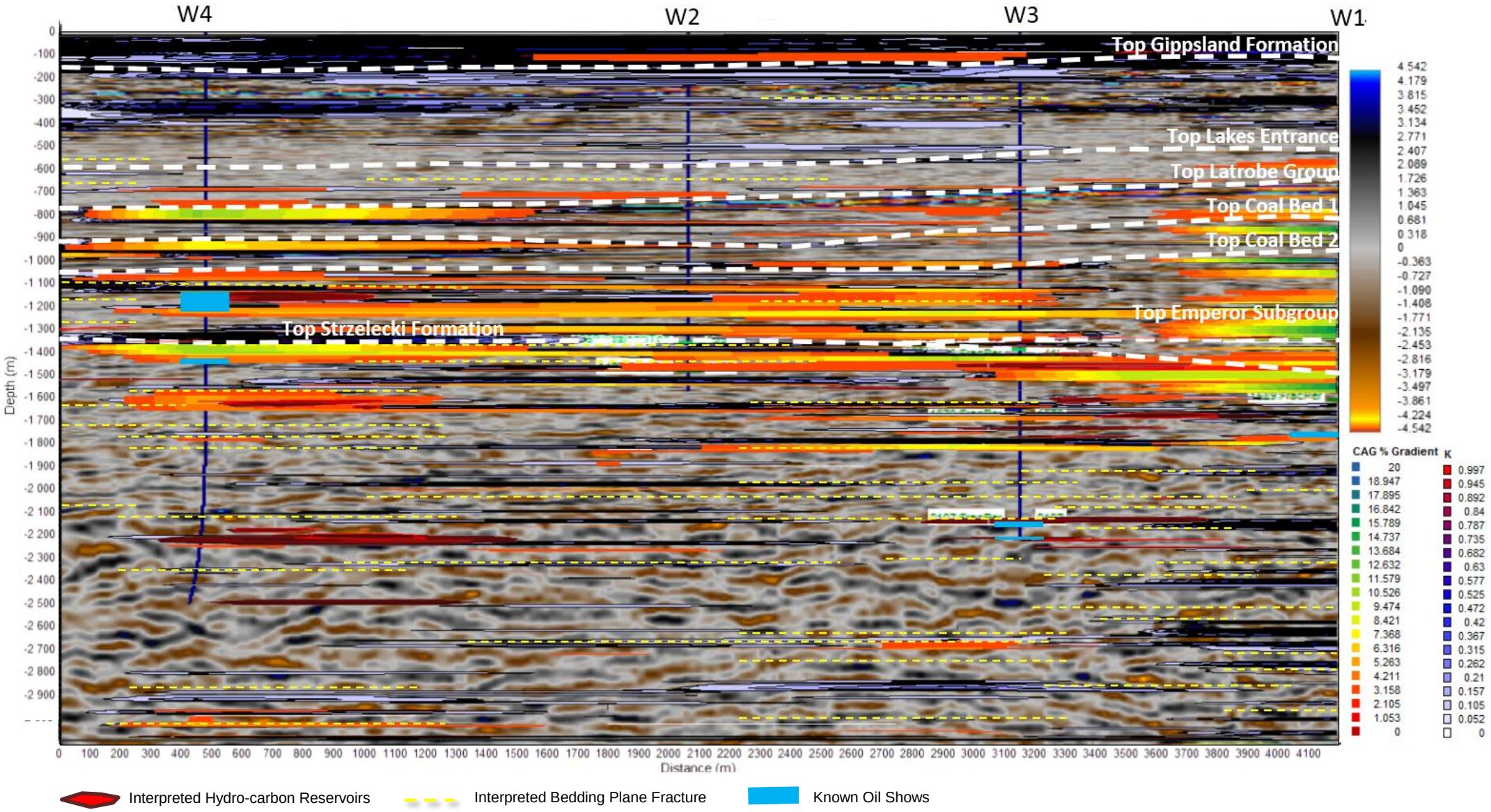

Figure 15 – ES Hydraulic Conductivity (ESKT), ES Fracture data (ESFT), ES Coupling Coefficient (ESCCT) and ES Change in Absolute Gradient Response (ESCAGT) to Seismic section and formation interface interpretation comparison

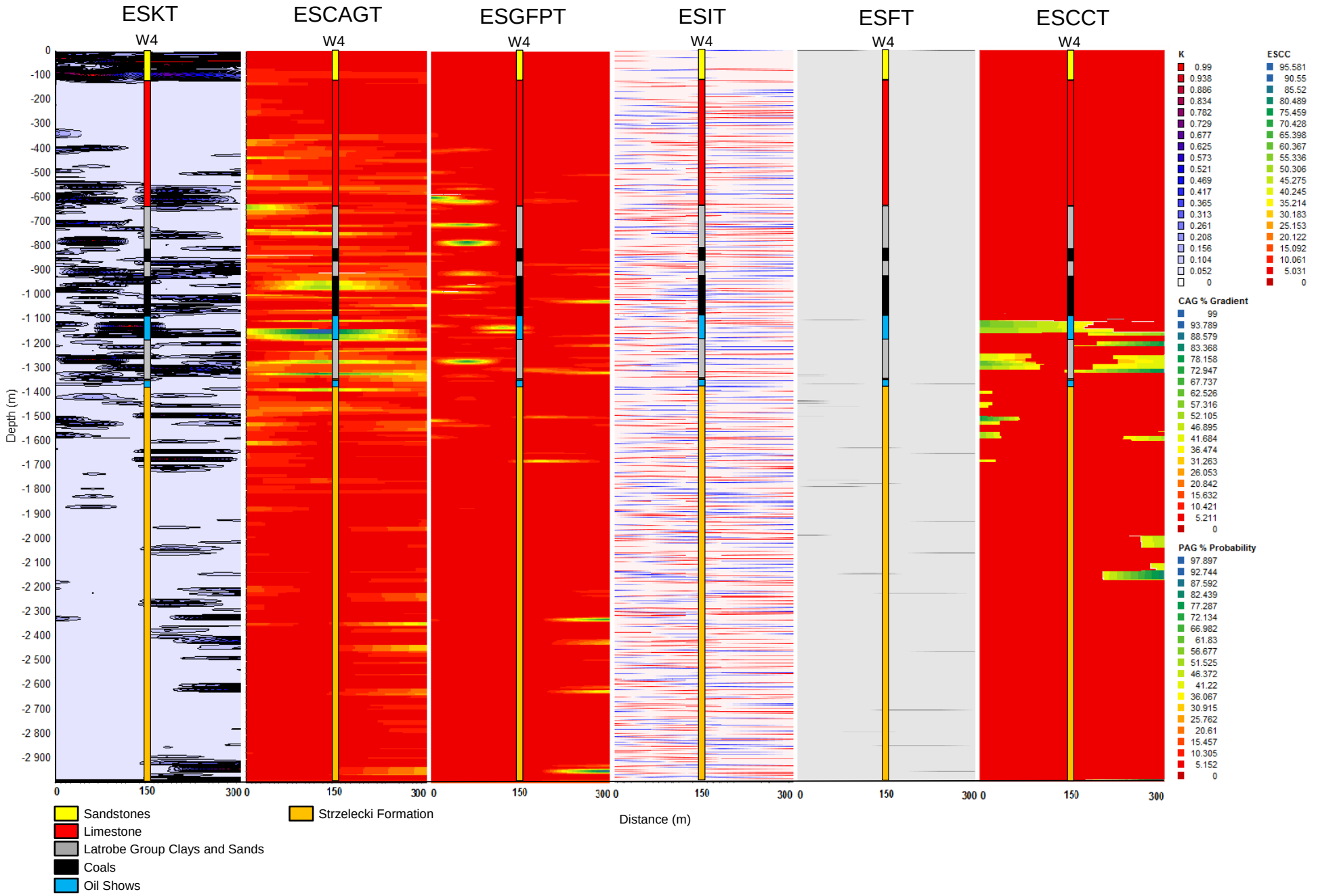

Figure 16 – High resolution grid 2D Section Data for the ESKT, ESCAGT, ESGFPT, ESIT, ESFT and ESCCT data set comparison against the Wombat 4 Geological and oil show logs

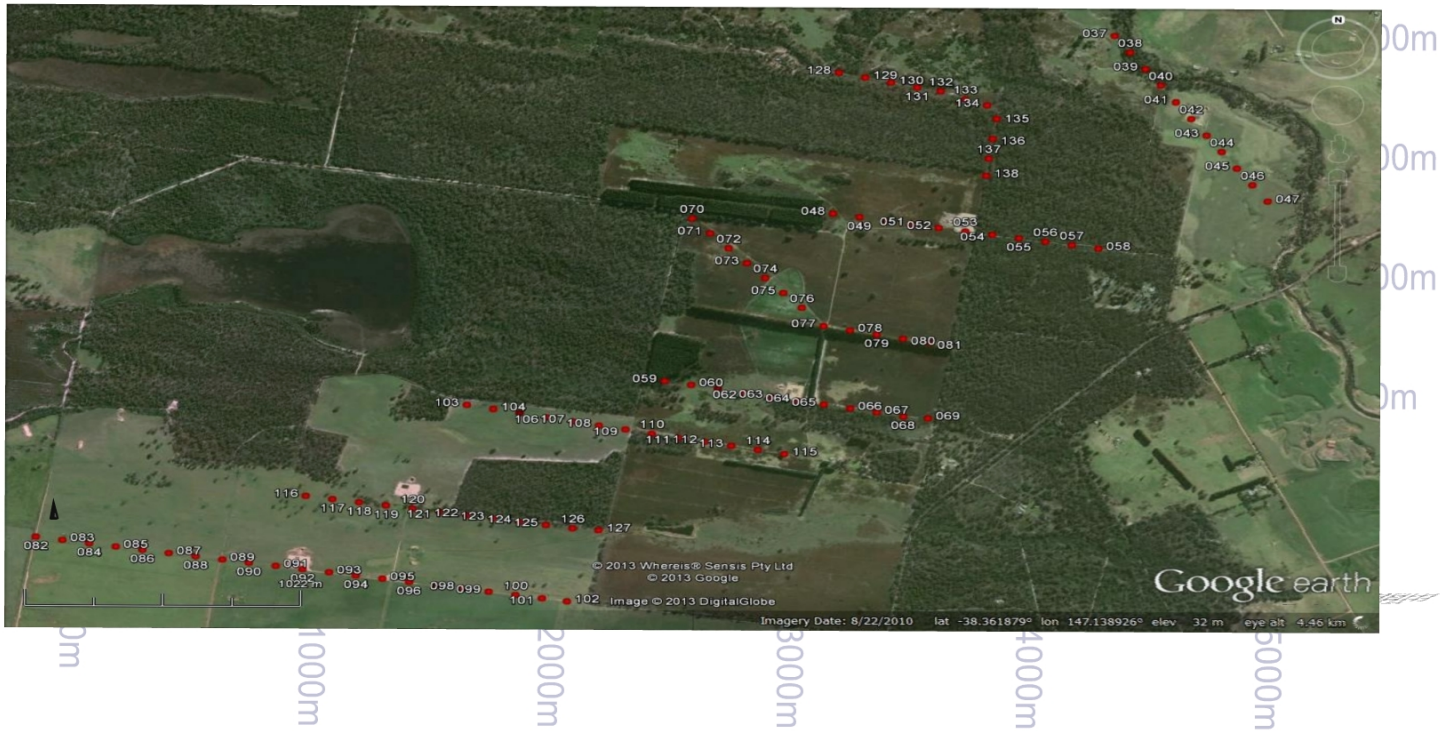

Figure 17 - 3D Model

10 Discussion of 2D results

10.1 Hydraulic Conductivity Results

The data shown in Figure 6 is set to a scale of 1 to 0 mm/day. The data indicates that there are two aquifer systems within the top Gippsland formation at 40m and 120m depth where the top aquifer appears to be the more permeable of the two. Beneath this is a formation that appears to be of low permeability. This formation extends to 650m depth and is confirmed to be a limestone formation. This is consistent with the low hydraulic conductivity values seen in Figure 6. There does however appear to be an area of higher hydraulic conductivity at a depth of 300m to 400m depth within the limestone formation. Beneath the limestone formation, the Latrobe group starts. It consists of a number of interbedded sandstones, marls, clays and coals. Defining the location of the known coal beds under the site is an objective of this study. It is expected that the coal seams would have significantly lower permeability than their surrounding formations. This is one of the characteristics used for delineating the coal seams within the Latrobe group. Clear areas of low permeability at 850m and 1000m depth can be seen in Figure 6. The presence of the coal bed interfaces is also seen in the ESCAGT data shown in Figure 6. This is discussed further on in this document. Indications of low permeability clays and higher permeability sandstones are also visible in the Latrobe.

The top of the Strzelecki formation follows on below the Latrobe group. It consist of a thin upper layer of high permeability weathered sandstone approximately 50m thick. This is followed by another 150m of semi-weathered sandstone. This semi-weathered zone also includes primary permeability lenses that may be due to hydraulic fracturing of the tight sands within this weathered Strzelecki formation. The un-weathered Strzelecki formation forms the base of the survey to a depth of 3000m. It consists of mostly very low permeability tight sands which is interbedded with lenses of higher permeability sands.

10.2 Electro Seismic Change in Absolute Gradient Response Tomography Results

As discussed in section 9.4, Figure 6 shows the electro seismic change in absolute response is used to differentiate absolute electrical changes in rock formation properties, in proportion to each other. The ESCAGT data shown in Figure 6 show strong responses at the interfaces between the coal seams and their neighbouring sandstone formations. This is to be expected due to the large variation in hydrological and electrical characteristics between the coal materials and the sandstone formations. This characteristic response of a coal sedimentary interface was used in conjunction with the low permeability found within the coal beds to determine their depth and thickness.

There is also a strong interface response at the juncture between the Latrobe group and the highly weathered upper layer of the weathered Strzelecki formation. This may be due to electrical property variations between the highly weathered sandstone and the lower permeability weathered sands below. This gives a clear horizon for the top of the Strzelecki formation.

There are a number of weaker responses that indicate the interface between the limestone / Latrobe formation at approximately 650m depth. This was used to define the interface throughout the sounding section.

10.3 Fracture Analysis Results

The bedding plain fracture data shown in Figure 8 indicates the presence of fracturing within the tight sands Strzelecki formation. The fracturing appears to be intense to the East of the site and the far West. This indicates the probable presence of faulting which may be the cause of the breaks. There are some indications of bedding plain fracturing in the upper limestone formations, however there is very little indications of fracturing within the Latrobe group. There is some indications of fracturing in the weathered Strzelecki formation, however most indicators appear to be in the deeper un-weathered Strzelecki formation. The largest concentration of fracturing occurs between1900m to 2300m depth to the East of the site.

10.4 Electro-Seismic Coupling Coefficient Tomography Results

Figure 8 also shows the ESCCT data set at a coefficient level of 0.99. This shows only the strongest of the ESCCT responses which indicate probability of high ground fluid salinity. Fluid salinity is an indicator of hydro-carbon reserves and in this case is the only indicator hydro-carbons. No major viscosity variation were detectable, indicating that the hydro-carbons reservoirs on site lie within very thin reservoirs or that the hydro-carbons are being transported within fracture networks. The information provided by the site well logs indicate that the hydro-carbons under the site are being transported by natural fracture networks. The presence of fault lines near the boundaries of the survey area indicate that these fracture networks may be transporting hydro-carbons from a greater depth than investigated in this study. The shape and location of the interpreted hydro-carbon bearing structures,

which are very thin in thickness and located mainly around the denser fracture network zones, support this supposition.

10.5 Electro Seismic Groundwater flow potential Tomography Results

The ESGFPT data, shown in Figure 9, indicates the areas that high probability of groundwater flow may cause water influx into drilled wells. The area of most concern is the highly weathered upper layer of Strzelecki sands which shows a clear horizon of groundwater flow reserve through the length of the sounding profile. This information can assist in the development of well casing designs for future well placements. It can also provide information to assist environmental studies.

10.6 Electro Seismic Geological Interpretation Results

All the discussed results were used to compile a geological interpretation for the ES profile section. This interpretation is shown in Figure 7. When compared to the interpretation provided by Lakes Oil, shown in Figure 5, a strong correlation is evident. The ES interpretation is more detailed as it includes permeability variation data which is described as specific geological units, such as sands, coals, clays etc.

10.7 Electro Seismic evaluation of the high resolution grid around Wombat 4

A short 2D section of ES survey data was generated across the high resolution grid around W4. This section can be seen in Figure 4 and the ES data for this section is shown in Figure 16. The data shown for the section indicated in Figure 4 runs from West to East. The high resolution ES survey data around well 4, shown in Figure 16, indicates the same geological and hydro-geological trends as the site overview data. Figure 16 shows the ESKT, ESCAGT, ESGFPT, ESFT and ESCCT data set show similar horizons when compared to the lower resolution grid overview. As the grid is of sufficient resolution to display ES interface tomography Data (ESIT) the data set is also included. These data sets are compared against the known geological well logs for W4 provided by Lakes Oil.

The ESKT data indicates the same hydrological responses discussed in the low resolution survey. The upper shallow aquifer systems are clearly visible. The Latrobe group sand aquifers are also visible. The low permeability coals are clearly visible as aquicludes.

The ESCAGT data indicates the strong formation responses at the interfaces between the coal beds and the surrounding sands. This is consistent with the finds of the lower resolution survey data.

The ESGFPT data is also consistent with the results shown in the low resolution grid results. There is a distinct flow probability horizon just above the Strzelecki formation.

The ESIT data shows the major geological formation interface under the site. Unfortunately the length of the shown profile section is too short to accurately determine major interface horizons.

The ESFT data shows the same fracturing trends as discussed in the low resolution grid assessment. The data indicates that most fracturing occur within the Strzelecki formation and lines up well with the oil reserve responses shown in the ESCCT data set.

The ESCCT data shows good correlation between the known oil shows shown in the well logs and the ESCCT oil estimates.

11 2D Comparative Study Results

11.1 Seismic Formation Interpretation

Figure 10 shows the seismic section data, provided by Lakes Oil, over the same cross section as the ES 2D data sets discussed previously. An interpretation of the seismic section geological formations as provided by Lakes Oil, is also shown in Figure 10 as a set of dotted white lines. The corresponding formation interface names are also shown. The seismic data clearly illustrates these interfaces as strong reflectors, as referenced by the colour scale provided. The Strzelecki formation is interpreted to be the last major formation change before the maximum investigation depth is exceeded. It is evident that the interpreted coal bed interfaces are strong seismic reflectors, as the seismic energy transmitted through these formations are drastically attenuated and the seismic reflects below the coals are not as pronounced. This makes the use of seismic data to interpret formations deeper than the coal beds less effective than what is ideally required.

11.2 Hydraulic Conductivity Comparison

Figure 11 shows the seismic section data, provided by Lakes Oil, over the same cross section as the ES 2D data sets discussed previously. An interpretation of the seismic section geological formations as provided by Lakes Oil, is also shown in Figure 11 as a set of dotted white lines. The corresponding formation interface names are also shown.

The ES Hydraulic Conductivity data (ESKT) is overlaid on top of the seismic data for comparison. The first and most evident observation, of the comparative data sets, is that the strong refection responses in the seismic data set correlates well with the higher hydraulic conductivity data for the ESKT data. This indicates that the strong seismic reflectors are being caused by the seismic transition between high permeability sands and lower permeability coals, clays or tight sands.

It is evident that ESKT data can be used to define the geological formation structure and interfaces between sandstones and lower permeability coals and clays. This is more prevalent, in this case study, for formation interfaces below the coals, as the seismic data does not indicate reflectors as strongly. An exception to this case is seen to the east of the profile, where strong seismic reflectors correlate well with the higher ESKT data sets at depth greater than 1600m.

The Latrobe Group between 1000m and 1300m depth shows significant permeability within two perceived permeable sandstone lenses at depths of 1100m and 1200m. This is not clearly visible as strong seismic reflectors, however, a strong correlation exists with the geological well logs of wells W4, W2 and W3.

There is also a strong indication of high permeability sands at the interface of the Strzelecki formation as interpreted from the seismic data set. This extends to a depth of approximately 1700m to the east of the site with lenses of higher permeability zones, indicating the extent of the weathered Strzelecki group. This can however not be confirmed by the seismic data set as there are no evident reflectors at this depth.

Within the perceived un-weathered Strzelecki formation there are correlations between the perceived higher permeability lens horizons and the higher intensity seismic reflectors. This could indicate the presence of higher permeability sands within the Strzelecki formation. This could be used in delineating gas production zones prior to well development.

It does appear that ES hydraulic conductivity data can add value to the interpretation of seismic data sets and the delineation of permeable formations.

11.3 ES Change in Absolute Response Gradient Comparison

Figure 12 shows the seismic section data, provided by Lakes Oil, over the same cross section as the ES 2D data sets discussed previously. An interpretation of the seismic section geological formations as provided by Lakes Oil, is also shown in Figure 12 as a set of dotted white lines. The corresponding formation interface names are also shown.

The ES Change in Absolute Response Gradient data (ESCAGT) is overlaid on top of the seismic data for comparison. The ESCAGT data shows interfaces where there are large differences in electrical characteristics between the geological formations that make up the interface. The ESCAGT data correlates well with the strong seismic reflectors, providing supporting evidence to the seismic interface interpretations. The ESCAGT data also highlights the base of the weathered Strzelecki formation. This is useful, as the weathered Strzelecki formation is not clearly visible in the seismic data set.

The top of the Gippsland formation and the top of the Latrobe Group is also clearly visible. However the top of the Lakes entrance is not. This may indicate that the limestone formation and the Lakes entrance group are not different in electrical terms, indicating that they consist of similar geologies.

There does not appear to be significant ESCAGT responses below the perceived weathered Strzelecki formation at approximately 1700m depth. This indicates that there are no major formation changes before the survey investigation limit of 3000m is exceeded.

It is important to note that seismic data relies on changes in the acoustic properties of the materials it passes through and does not account for any geological electrical changes. ES methods account for both electrical and acoustic property changes and as such is capable of delineating these electrical changes in geological formations. As such, the use of ECAGFT data can provide a completely different aspect of interpretation that seismic information cannot provide.

11.4 ES Bedding Plane Fracture Comparison

Figure 13 shows the seismic section data, provided by Lakes Oil, over the same cross section as the ES 2D data sets discussed previously. An interpretation of the seismic section geological formations as provided by Lakes Oil, is also shown in Figure 13 as a set of dotted white lines. The corresponding formation interface names are also shown.

The ES bedding plane fracture data (ESFT) is overlaid on top of the seismic data for comparison. There does not appear to be any significant correlation between the ESFT data and the seismic data. This indicates that the seismic

data cannot be used to delineate bedding plain fracturing, in this case study. In this case, the use of ESFT data can provide a completely different aspect of interpretation that seismic information cannot provide.

11.5 ES Hydro-Carbon Reservoir Comparison

Figure 13 shows the seismic section data, provided by Lakes Oil, over the same cross section as the ES 2D data sets discussed previously. An interpretation of the seismic section geological formations as provided by Lakes Oil, is also shown in Figure 13 as a set of dotted white lines. The corresponding formation interface names are also shown.

The ES Coupling Coefficient data (ESCCT) is overlaid on top of the seismic data for comparison. The ESCCT data for a threshold value of 0.99 is shown in Figure 13, as it illustrates only the areas of highest fluid salinity. This is done as high salinity fluids are strongly associated with hydro-carbon reserves.

It is evident that the seismic data does not show any discernable correlation with the ESCCT data. This is not unexpected as seismic data relies only on changes in the acoustic properties of the materials it passes through and does not account for any geological or fluidic electrical changes. ES methods account for both electrical and acoustic property changes and as such is capable of delineating these saline fluids.

The known oil shows, taken from well log data provide by Lakes Oil, are indicated on Figure 13. There is correlation between the ESCCT and the oil show data. This indicates that the ESCCT can be used to effectively delineate hydro-carbon resources to depths up to 2200m.

Once again, in this case, the use of ECCFT data can provide a completely different aspect of interpretation that seismic information cannot provide.

11.6 ES Groundwater Flow Potential Comparison

Figure 14 shows the seismic section data, provided by Lakes Oil, over the same cross section as the ES 2D data sets discussed previously. An interpretation of the seismic section geological formations as provided by Lakes Oil, is also shown in Figure 14 as a set of dotted white lines. The corresponding formation interface names are also shown.

The ES Groundwater Flow Potential data (ESGFPT) as well as the ES Hydraulic conductivity data (ESKT) is overlaid on top of the seismic data for comparison.

The data indicates that the highest probability for groundwater flow lies within the higher permeability sands at the interface of the Latrobe and Strzelecki formations. This is useful when anticipating potential problem areas when planning well designs.

11.7 Overall ES data to Seismic Section Comparison

Figure 15 shows the seismic section data, provided by Lakes Oil, over the same cross section as the ES 2D data sets discussed previously. An interpretation of the seismic section geological formations as provided by Lakes Oil, is also shown in Figure 15 as a set of dotted white lines. The corresponding formation interface names are also shown.

The ESKT, ESCAGT, ESCCT and ESFT data is overlaid on top of the seismic data for a full comparison.

The data shows correlation between the strong seismic reflectors and the ES hydraulic conductivity responses as well as the ESCAGT data. Even at depths below 2000m, there is correlation between the ES and Seismic data sets. This indicates that ES methods can be used to support seismic investigation. The ESCCT and ESFT data do not show strong correlation. This may be due to limitations of seismic methods at delineating bedding plain fracture networks and electrical variations in fluids within the subsurface.

This methodology should be further studied to define the relationships between ES and seismic responses more clearly. It is evident that the two methods can be used to support each other's findings and will allow a geophysicist to better describe a survey sites geology and geo-hydrology.

12 Discussion of 3D results

12.1 Hydraulic Conductivity results

The "Hydraulic Conductivity 0.5 mm/Day" view in the 3D model, shown in Figure 17, illustrates the hydraulic conductivity Iso-surface data for the study site set at a value of 0.5 mm/day. The data closely reflects the data for the 2D section profile previously discussed. The distinct sandstone aquifers within the Gippsland formation are clearly visible as two distinct horizons at 40m and 120m depth. These two aquifer systems appear to run beneath the entire area of the survey site. The aquifer within the limestone formation between 300m and 400m is also clearly visible. This aquifer also seems to run beneath the entire length of the survey

area. The distinct aquiclude that is part of the limestone formation indicates that no visible hydrological connection exists between the upper aquifers and the aquifer systems below the limestone formation.

The start of the Latrobe Group at approximately 650m depth, shows the higher permeability's of the sandstone formations that lie above, in between and below the very low permeability coal formations.

The top of the Strzelecki formation is also visible as a distinct drop in hydraulic conductivity between 1300m and 2800m depth. This is very evident below 1600m depth indicating the presence of the known weathered Strzelecki layer on top of the un-weathered Strzelecki formation. There are also indication of higher permeability lenses within the un-weathered Strzelecki formation. There are some indications of higher permeability formations at depths of 2800m to 3000m depth, however, they cannot be confirmed due to the lack of geological data at those depths.

There appears to be high permeability formations between 2000m and 2700m depth to the north east of the site. This may be due to the influence of primary of secondary faulting in this area. The higher permeability responses do coincide with strong seismic reflectors at those depth as seen in Figure 10.

The "Hydraulic Conductivity 0.05 mm/Day" view in the 3D model, shown in Figure 17, illustrates the hydraulic conductivity Iso-surface data for the study site set at a value of 0.05 mm/day. This view is limited to a depth zone of 1000m to 1600m depth to investigate the weathered zone that forms part of the Strzelecki formation. The data indicates that there is a distinct drop in permeability from the bottom Latrobe formation to the top of the Strzelecki formation. The Latrobe sandstones are more permeable than the weathered Strzelecki formation. This is reflected in the well logs as well. The weathered Strzelecki formation permeability's seem to be variable in both the vertical and horizontal plain, although there does appear to be a highly permeable transition between the Latrobe and the Strzelecki formations.

12.2 Electro seismic change in Absolute Gradient Response

The "Structural Analysis" view in the 3D model, shown in Figure 17, illustrates the ESCAGT Iso-surface data for the study site. The data mirrors the 2D data set shown in Figure 6 and illustrates the positions of the coal bed interfaces, the Latrobe group interface and the Strzelecki interface.

12.3 Fracture Analysis

The "Bedding Plain Fracturing" view in the 3D model, shown in Figure 17, illustrates the ES fracturing analysis Iso-surface data for the study site. The data clearly shows two distinct fracture zones to the south west and the north east of the site. This is also evident in the 2D analysis data shown in Figure 8. These fracture networks groups are highly localised and indicate geological faulting deformations as a possible cause of this secondary permeability.

12.4 Vertical Structure Analysis

The "Vertical structure interpretation" view in the 3D model, shown in Figure 17, illustrates the ES vertical structure analysis Iso-surface data for the study site. This interpretation of the perceived secondary structures is done using the fracture network analysis, previously discussed. This interpretation assumes that the fracture groups are caused by secondary effects of faulting in the area of the fracture groups. Linear faulting plains are approximated using the bedding plain fracture analysis results as a guide and overlaid on the bedding plain fracture data.

12.5 Hydro-carbon Reserve Analysis

The "Interpreted Hydro-carbon reserves" view in the 3D model, shown in Figure 17, illustrates the ES hydro-carbon reserve analysis Iso-surface data for the study site. The hydrocarbon reserves are also grouped into two distinct zones that correlate well with the fracture and interpreted fault line groups.

The "Interpreted Hydro-carbon feeds" view in the 3D model, shown in Figure 17, illustrates the ES hydro-carbon feed analysis Iso-surface data for the study site. This data set overlays the hydro-carbon reserve data on top of the vertical structure analysis data. The correlation between the two data sets indicate that the hydro-carbons in the survey area are located within fracture networks created by fault lines. This indicates that the hydro-carbon reserves are limited and are being sourced from a deeper reservoir through natural fault lines and fracture networks.

12.6 Potential Groundwater flow regions

The "Potential groundwater flow zones" view in the 3D model, shown in Figure 17, illustrates the ES groundwater flow analysis Iso-surface data for the study site. The data indicates that there are limited zones where groundwater flow could affect the design of a gas well.

12.7 Fine Grid Fracture analysis

The “Fine Grid Fracture Analysis” view in the 3D model, shown in Figure 17, illustrates the ES fracture analysis Iso-surface data for the fine grid study site around Wombat 4 well. The grid spacing for this grid is 50 x 50m and the total grid sixe is 300m x 300m. This is a significantly higher resolution grid than the general site survey grid. The purpose of this survey is to determine the state of the natural fracture networks around W4 before the hydraulic fracturing of the tight sands in the Strzelecki formation affects the secondary permeability of the site. A comparison of the survey before fracturing, and one after fracturing has taken place, will indicate if ES methods can detect the extent of hydraulic fracturing effects on the Strzelecki formation. The data indicates that there is very little natural fracturing around W4, which is consistent with the W4 geological well log. Another ES survey will be done around the W4 well after hydraulic fracturing has taken place and compared to this data set in order to determine secondary permeability enhancements under the site.

13 Conclusions

It is evident that electro-seismic methods can be used to geologically and hydrologically define unconventional oil and gas tight sands sites. The study also indicates that hydro-carbons within fracture networks can be defined using ES methods. It is also evident that comparative studies between seismic and electro-seismic data can be beneficial to the understanding of a sites geology and hydro-geology.

14 Recommendations

If the depth of the investigation is to be improved, the survey must be re-conducted with dry site conditions to limit the seismic absorption effects of soft top soils. To improve the results of the general overview, a higher resolution grid can be used to improve resolution and clarity of the model.ATS highly recommend that several high resolution lines be shot over the planned area of Wombat 5. This will allow a higher resolution and targets approach to drilling the well and also will assist with well planning and consenting process required to drill the well.

15 References

1. Biot, M. A. (1956) Theory of propagation of elastic waves in a fluid-saturated porous solid. I. Low frequency range. *Journal of the Acoustical Society of America.*

2. Biot, M. A. (1956) Theory of propagation of elastic waves in a fluid-saturated porous solid. II. Higher frequency range. *Journal of the Acoustical Society of America.*

3. Biot, M. A. (1962) Generalized theory of acoustic propagation in porous dissipative media. *Journal of the Acoustical Society of America.*

4. Botha, J. F., Verwey, J. P., Van der Voort, I., Vivier, J. J. P., Colliston, W. P. and Loock, J. C. (1998) *Karoo Aquifers. Their Geology, Geometry and Physical Behaviour*. Water Research Commission.

5. Butler, K. E., Russell, R. D. and Kepic, A. W. (1996) Measurement of the seismoelectric response from a shallow boundary. *Geophysics.*

6. Fourie, F. D. (2000) *An Introduction to Geophysics for Geohydrologists*. Unpublished lecture notes. Institute for Groundwater Studies, University of the Orange Free State.

7. Garambois, S. and Dietrich, M. (2001) Seismo-electric wave conversion in porous media: Field measurements and transfer function analysis. *Geophysics.*

8. Haartsen, M. W. and Pride, S. R. (1997) Electroseismic waves from point sources in layered media. *Journal of Geophysical Research.*

9. Haartsen, M. W., Dong, W. and Toksöz, M. N. (1998) Dynamic streaming currents from seismic point sources in homogeneous poroelastic media. *Geophysical Journal International.*

10. Ishido, T. (1981) Experimental and theoretical basis of electrokinetic phenomena in rockwater systems and its application to Geophysics. *Journal of Geophysical Research.*

11. Kepic, A. W., Maxwell, M. and Russell, R. D. (1995) Field trials of a seismoelectric method for detecting massive sulphides. *Geopysics.*

12. Martner, S. T. and Sparks, N. R. (1959) The electroseismic effect. *Geophysics.*

13. Maxwell, M., Russell, R. D., Kepic, A. W. and Butler, K. E. (1992) Electromagnetic responses from seismically

excited targets B: Non-piezoelectric phenomena. *Exploration geophysics.*

14. Mikhailov, O. V., Haartsen, M. W. and Toksöz, M. N. (1997) Electroseismic investigation of the shallow subsurface: Field measurements and numerical modelling. *Geophysics.*

15. Millar, J. W. A. and Clarke, R. H. (1997) *Electrokinetic techniques for hydrogeological site investigations*. Groundflow

16. Pride, S. R. (1994) Governing equations for the coupled electromagnetics and acoustics of porous media.

17. Pride, S. R. and Haartsen, M. W. (1996) Electroseismic wave properties. *Journal of the* Acoustical Society of America.

18. Pride, S. R. and Morgan, F. D. (1991) Electrokinetic dissipation induced by seismic waves. Geophysics.

19. Ranada Shaw, A., Denneman, A. I. M. and Wapenaar, C. P. A. (2000) Porosity and permeability effects on seismo-electric reflection. In: Proceedings of the EAGE conference.

20. Russell, R. D., Butler, K. E., Kepic, A. W. and Maxwell, M. (1997) Seismoelectric exploration. The Leading Edge.

21. Rosenberg, M., Wallin, E., Bannister, S., Bourguigon, S., Jolly, G., Mroczek, E., Milicich, S., Graham, D., Bromley, C., Reeves, R., Bixley, P., Clothworthy, A., Carey, B., Climo, M. (2010) Tauhara Stage || Geothermal Project: Geoscience Report, GNS Science Consultancy Report 2010/138.

22. Du Preez, M. (2005) Accuracy of Electro-Seismic Techniques Applied to Groundwater Investigations in Karoo Formations. Master Thesis: University of the Free State